

# Synthesis and properties of novel biodegradable polyurethanes containing fluorinated aliphatic side chains

Shuenn-Kung Su<sup>1</sup> · Jia-Hao Gu<sup>1</sup> · Hsun-Tsing Lee<sup>2</sup> · Cheng-Lung Wu<sup>1</sup> · Jiunn-Jer Hwang<sup>3</sup> · Maw-Cherng Suen<sup>4</sup>

Received: 14 February 2017 / Accepted: 6 August 2017 / Published online: 17 August 2017  
© Springer Science+Business Media B.V. 2017

**Abstract** This study used 5H-octafluoropentanoylfluoride and 2-amino-2-methyl-1,3-propanediol to synthesize a novel fluoro chain extender 2,2,3,3,4,4,5,5-octafluoro-N-(1,3-dihydroxy-2-methylpropan-2-yl) pentanamide (ODMP). Furthermore, 4,4'-diphenylmethane diisocyanate served as the hard segment, polycaprolactone diol (PCL) served as the soft segment, and ODMP served as the chain extender in the novel synthesized polyurethanes (ODMP/PUs). Gel permeation chromatography revealed that the molecular weight of the ODMP/PUs increased when the ODMP content was increased. <sup>1</sup>H and <sup>19</sup>F nuclear magnetic resonance and Fourier transform infrared spectroscopy verified that the ODMP chain extenders were successfully synthesized and that the ODMP chain extenders were successfully incorporated into the backbone of the PUs. The interaction between the -NH (hydrogen bond) and CF<sub>2</sub> groups in the ODMP/PUs became stronger when the ODMP content was increased. Thermal analysis revealed that the initial decomposition temperature of the ODMP/PUs decreased and the second decomposition temperature increased when the polymers' ODMP content was increased. Higher ODMP content also resulted in the ODMP/PUs' higher glass

transition and dynamic glass transition temperatures and lower ODMP maximum stress and Young's modulus, causing a lower elongation at break. ODMP/PUs with higher ODMP content exhibited more protrusions and more rugged surfaces. The chemical resistance of the ODMP/PUs increased when the fluorine content was increased. Scanning electron microscopy revealed that ODMP/PUs with higher PCL content exhibited higher levels of hydrolytic degradation. Finally, in vitro erythrocyte tests revealed that increasing the ODMP chain extender content reduced the average number of erythrocytes adhering to the surface of the PUs.

**Keywords** Polyurethanes · Chain extender · Chemical resistance · Hydrolytic degradation · Erythrocyte adhesion

## Introduction

Polyurethane (PU) is generally formed by reacting diisocyanate with long chain polyols and short chain extenders [1]. Elastomers with various properties can be synthesized by combining soft and hard segments in different ratios. Because it can be particularly elastic, PU is widely used in fibers, foam plastics, artificial leather, paints, and adhesives, thus serving as an indispensable material in multiple industries [2–6]. However, conventional PU materials generally have a few drawbacks such as unsatisfactory heat resistance or biocompatibility, thereby restricting their possible application in various areas. Fluorocarbon chains have numerous unique and interesting properties including excellent oxygen permeability; small dielectric constant; favorable hydrolytic stability, thermal stability, and chemical resistance; low interfacial free energy; and satisfactory oil resistance [7–9].

Ample research has been conducted on PUs containing fluorine units and has identified excellent unique properties of such

✉ Maw-Cherng Suen  
sunmc0414@gmail.com

<sup>1</sup> Department of Materials Science and Engineering, National Taiwan University of Science and Technology, Taipei Taiwan 10607, Republic of China

<sup>2</sup> Department of Materials Science and Engineering, Vanung University, Jongli, Taoyuan Taiwan 32061, Republic of China

<sup>3</sup> Department of Chemical Engineering, Army Academy, Jongli, Taoyuan Taiwan 32092, Republic of China

<sup>4</sup> Department of Fashion Business Administration, LEE-MING Institute of Technology, No. 22, Sec. 3, Tailin. Rd., New Taipei City Taiwan 24305, Republic of China

materials such as their superior chemical resistance and thermal stability, low surface tension and surface adhesion, and small dielectric constant [10–13]. PUs can be incorporated with fluorinated hard segments [14, 15], fluoro chain extenders [16–20], and soft segments [21–26] using various methods. For example, Ho et al. synthesized a series of fluorinated PUs using various fluorinated diols and determined that PU exhibits minimal surface adhesion [12, 13]. Tonelli adopted perfluoropolyethers as soft segments to synthesize fluorinated PU that had a small surface friction coefficient, satisfactory thermal stability, and excellent chemical resistance [23, 24]. Kashiwagi et al. synthesized PU that contained a fluoroalkyl group in the side chain of its hard segment, discovering that the formation of *in vitro* thrombus decreased when its fluoroalkyl group content increased [15]. In recent years, overuse of resins has caused numerous environmental issues, such as pollution to the natural environment and the fast exhaustion of oil reserves. Therefore, the development of renewable energies and biodegradable polymers has become a key issue [27–29]. Biodegradable PUs are generally produced using highly hydrolytic soft segments. These PUs typically exhibit biocompatibility, water solubility, and a low melting point or low crystallinity [30–34]. Compared with conventional polymers, these types of environmentally friendly polymer reduce waste while maintaining superior physical properties and biocompatibility [35–38]; therefore, numerous studies have been performed on them [39, 40]. Tsou et al. used polycaprolactone diol (PCL) as soft segments and 4,4'-diphenylmethane diisocyanate (MDI) and 2,6-pyridinedimethanol as hard segments to synthesize PUs. The results revealed that increasing the hard segment content enhanced the thermal resistance and mechanical properties of the PUs; conversely, lowering the PCL and hard segment content led to the improved hydrolytic degradability of the PUs [29].

In this study, a new fluorinate chain extender (2,2,3,3,4,4,5,5-octafluoro-N-(1,3-dihydroxy-2-methylpropan-2-yl) pentanamide [ODMP]) was synthesized through amidation of 5H-octafluoropentanoyl (OFF) and 2-amino-2-methyl-1,3-propanediol (AMPD). Subsequently, PCL and MDI were transformed into PU prepolymers. ODMP chain extenders were then added to produce ODMP/PUs polymers. The effect of the PCL segments and ODMP chain extenders on the structure, molecular weight, thermal properties, mechanical properties, and hydrolytic degradability of the PUs are reported. Furthermore, the preliminary blood compatibility of the PUs was evaluated through *in vitro* erythrocyte adhesion experiments.

## Experimental

### Materials

5H-octafluoropentanoyl fluoride (OFF), 2-amino-2-methyl-1,3-propanediol (AMPD), 4,4'-diphenylmethane diisocyanate

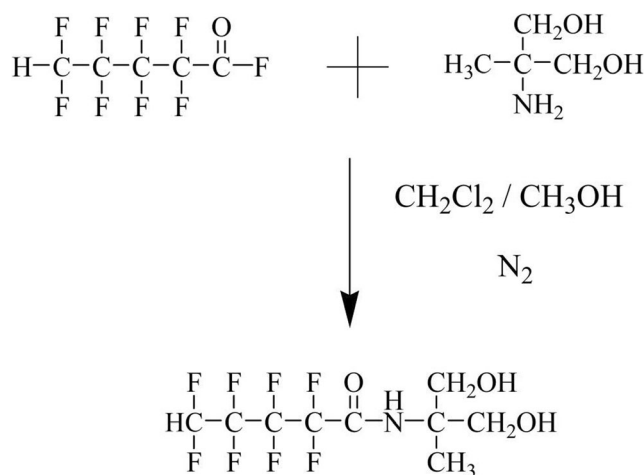
(MDI), polycaprolactone diol (PCL, (Mw = 530 g/mol), dibutyltin dilaurate (DBTDL), and dichloromethane were purchased from Aldrich. Methanol and N,N-dimethylacetamide (DMAc) were obtained from Mallinckrodt Chemicals.

### Synthesis of ODMP

OFF (in different amounts) and 80 mL of dichloromethane were added to a 500- mL flat-bottomed flask. At room temperature, nitrogen was bubbled through the mixture and stirred until complete dissolution. AMPD was then dissolved in methanol. The AMPD solution was syringed into the OFF solution at a mole ratio of 1:1. The solvents were removed using a rotary evaporator. The specimen was then dried for 12 h at 70 °C using a vacuum oven. The ODMP product thus acquired was then separated using column chromatography to obtain white crystals. Pure ODMP was then obtained by vacuum drying and subsequent drying at 50 °C in an oven for 1 day. The reaction formula for producing ODMP is presented in Scheme 1. <sup>1</sup>H NMR (DMSO-d<sub>6</sub>, Fig. 1) δ ppm a: 6.94 (m, 1H, Ha), b: 3.40 (m, 4H, Hb), c: 1.08 (s, 3H, Hc). <sup>19</sup>F NMR (DMSO-d<sub>6</sub>, Fig. 2) δ ppm –138.98, –130.97, –121.19, and –116.65. MS(EI): m/s 333.06 [M<sup>+</sup>], Calcd. 333.06. Anal. Calcd for C<sub>9</sub>H<sub>11</sub>F<sub>8</sub>NO<sub>3</sub>: C, 32.44% H, 3.33% N, 4.20%, Found: C, 32.40% H, 3.32% N, 4.18%.

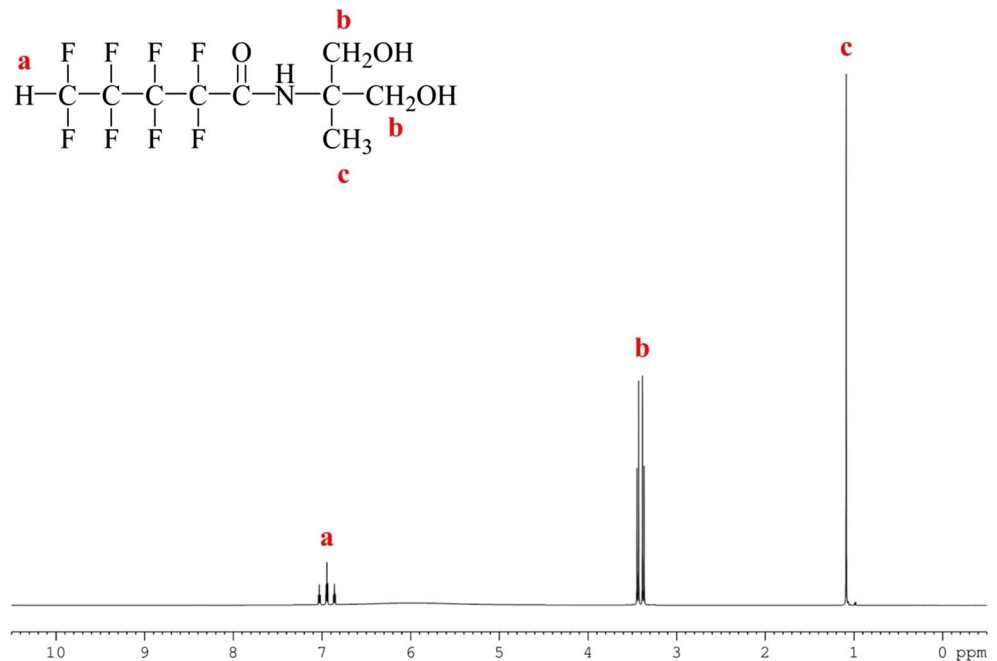
### Synthesis of ODMP/PUs

MDI, PCL, and DMAc were added to a 500-ml three-necked reaction flask and heated to 80 °C. A mechanical mixer was employed to mix the ingredients at 200 rpm. After 2 h of reaction, a PU prepolymer was formed. The ODMP chain extenders were dissolved in DMAc and added to the reaction flask for the second round of reactions for 2 h (Scheme 2). The obtained ODMP/PUs were poured into a serum bottle and placed in a refrigerator for 1 day. Finally, the ODMP/PUs



**Scheme 1** Synthesis formula for the ODMP

**Fig. 1** <sup>1</sup>H NMR spectra of the ODMP



solution was poured onto a Teflon plate and placed in a temperature-programmable circulating oven to dry for 8 h. Formula, symbols, and hard and soft segment content of the ODMP/PUs films are listed in Table 1. The hard and soft segment content was calculated using the following equations:

Hard segment content (wt%)

$$= \left( \frac{W_{ODMP}}{M_w_{ODMP}} \right) \times \left( \frac{M_w_{ODMP} + M_w_{MDI}}{W_{MDI} + W_{PCL} + W_{ODMP}} \right) \quad (1)$$

Soft segment content (wt%)

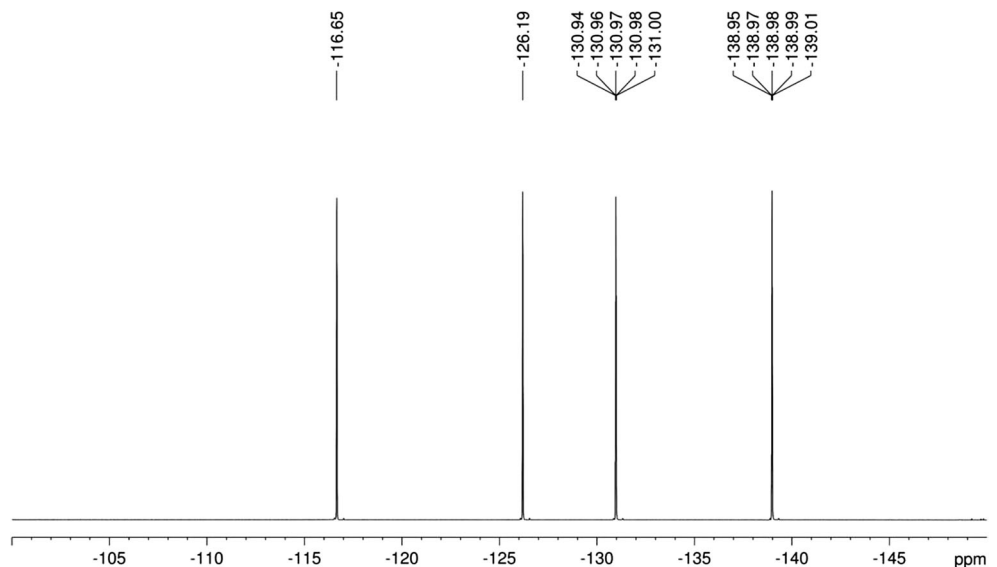
$$= 100\% - \text{Hard segment content (wt\%)} \quad (2)$$

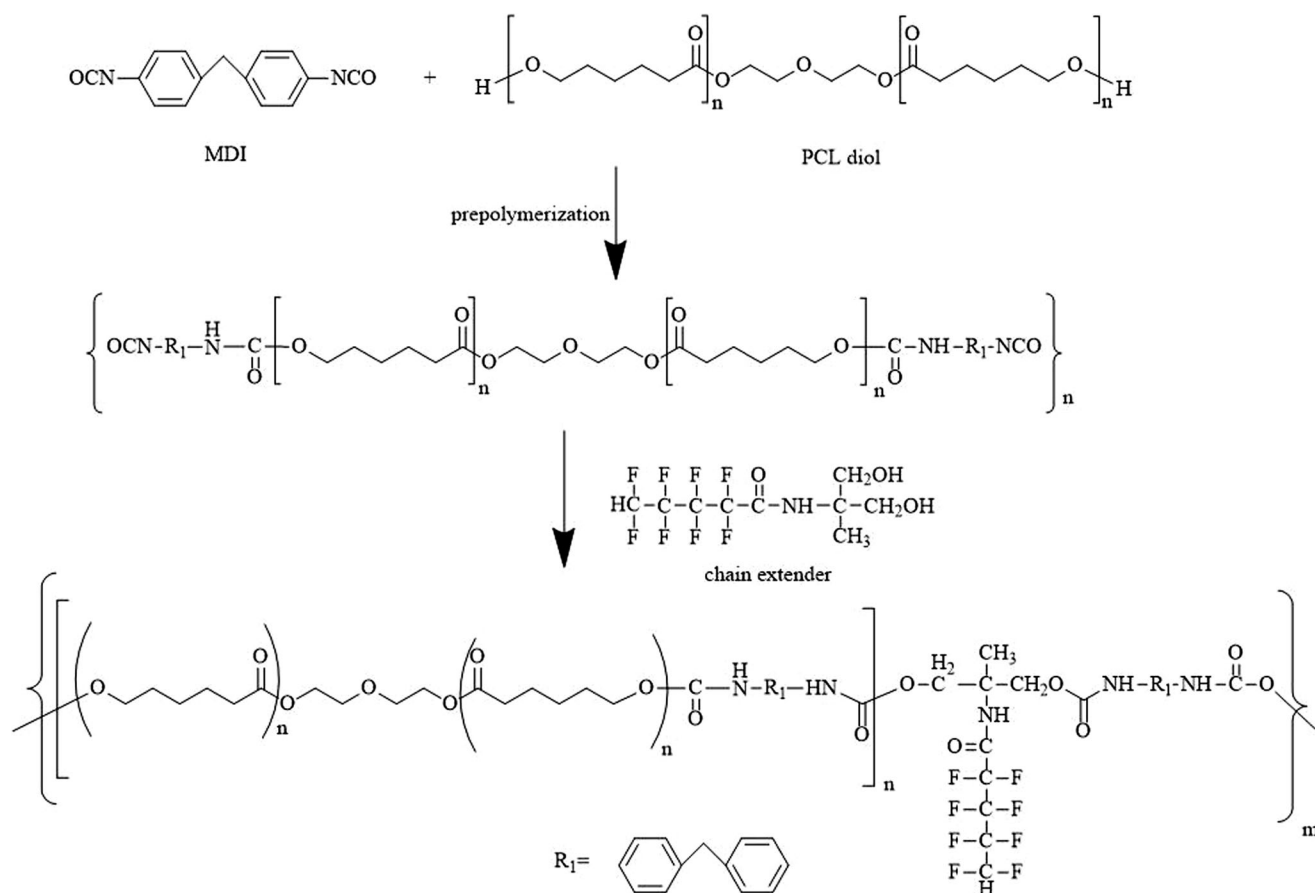
where  $W_{MDI}$  is the MDI weight,  $W_{PCL}$  is the PCL weight, and  $W_{ODMP}$  is the ODMP weight.

**Gel permeation chromatography (GPC)**

GPC was performed using Analytical Scientific Instruments' Model 500. A reflection index detector (Schambeck RI2000), two columns in a series of Jordi gel DVB mixed beds, and a 10,000 Å bed at 30 °C were used to measure molecular weight distributions relative to polystyrene standards. Eight standards with molecular weights ranging from 3420 to  $2.57 \times 10^6$  were

**Fig. 2** <sup>19</sup>F NMR spectra of the ODMP





**Scheme 2** Synthesis formula for the ODMP/PUs

used to perform corrections. The solvent used was tetrahydrofuran at a flow rate of 1 mL/min.

### $^1\text{H}$ NMR spectrometer

The  $^1\text{H}$  NMR (in DMSO- $d_6$ ) spectra of the specimens were measured using a Bruker Avance 300 spectrometer (300 MHz).

### $^{19}\text{F}$ NMR spectrometer

The  $^{19}\text{F}$  NMR spectra of the polymers were recorded using a Bruker Avance III HD 400 Hz spectrometer using DMSO- $d_6$  as a solvent and tetramethylsilane as an internal standard.

### Fourier transform infrared spectroscopy (FT-IR)

A PerkinElmer spectrometer (Model Spectrum One) was used to perform FT-IR. The specimens were scanned for an average of 16 times per  $4000\text{--}650\text{ cm}^{-1}$  at a resolution of  $2\text{ cm}^{-1}$ .

### X-ray photoelectron spectroscopy (XPS)

A Thermo Fisher Scientific (VGS) spectrometer was used to perform XPS. An Al  $K\alpha$  anode served as the X-ray source (1486.6 eV), and a binding energy range of  $0\text{--}1400\text{ eV}$  was analyzed. The binding energies were calibrated to the C 1s internal standard with a peak at 284.8 eV. The high-resolution C 1s spectra were decomposed by fitting a Gaussian function to the experimental curve using nonlinear regression.

**Table 1** Formulas of the ODMP/PUs

| Sample     | MDI (moles) | PCL (moles) | ODMP (moles) | Hard segment (wt%) | Soft segment (wt%) |
|------------|-------------|-------------|--------------|--------------------|--------------------|
| ODMP/PU-01 | 4           | 3.5         | 0.5          | 14.28              | 85.72              |
| ODMP/PU-02 | 4           | 3.0         | 1.0          | 29.52              | 70.48              |
| ODMP/PU-03 | 4           | 2.5         | 1.5          | 45.83              | 54.17              |

### Thermogravimetric analysis (TGA)

A PerkinElmer TGA device (model Pyris 1) was used for TGA. The specimens weighed 5–8 mg and were heated from room temperature to 700 °C at a heating rate of 10 °C/min.

### Differential scanning calorimetry (DSC)

A PerkinElmer calorimeter (model Jade) was used to perform DSC. The specimens were sealed in aluminum plates. In a nitrogen atmosphere, the scanning temperature was increased from –40 to 40 °C at a heating rate of 10 °C/min. The glass transition temperature ( $T_g$ ), the midpoint of the curve slope, was recorded. All specimens weighed 5–8 mg.

### Dynamic mechanical analysis (DMA)

A SEIKO device (model SII Muse, DMS6100) was used to perform DMA. Measurements were conducted under a tension mode with 1-Hz frequency and 5- $\mu$ m amplitude. The temperature was increased from –50 to 50 °C at a heating rate of 3 °C/min. The specimen dimensions were 20 × 5 × 0.2 mm<sup>3</sup> (L × W × H).  $T_g$  was calculated as the peak temperature of the glass transition region in the tan  $\delta$  curve.

### Stress–strain testing

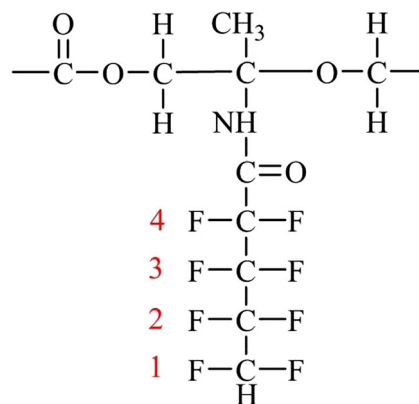
Tensile strength and elongation at break were measured using a universal testing machine (MTS QTEST5, model QC505B1). The testing was conducted according to ASTM D638 standards. The dimensions of the tested films were 45 × 8 × 0.2 mm<sup>3</sup>.

### Contact angle analysis

A face instrument (model CA-VP150) was used to measure the contact angle between specimens and deionized water at room temperature. A syringe pump was used to drop water on specimen surfaces. The contact angle was then recorded. Each contact angle was obtained by averaging the obtained angles over 3–4 drops.

### Surface roughness analysis

A CSPM5500 atomic force microscope from Being Nano-Instruments was used for scanning. The microscope features tapping and contact modes; the tapping mode was employed in this study. The two arms of the probe were oscillated to produce intermittent contact between the tip and the specimens. The tip oscillation phase was hypersensitive to various characteristics of the specimens. In addition to its topographical characteristics, the tip could detect phase images on



**Scheme 3** Structure of the ODMP/PUs

specimen surfaces. The specimens tested were ODMP/PU films containing various proportions of ODMP chain extender.

### Chemical resistance

Chemical resistance tests were conducted in accordance with the ASTM D1308 standard. Completely dry specimens (10- $\mu$ m thick) were placed in a sealed box containing various solvents. The solvents were removed after 24 h. The chemical resistance of the polymers was determined through visual inspection of the surface appearance of the films. The results of this visual inspection were expressed as follows: 5 (not affected), 4 (matte surface), 3 (softened), 2 (cracks), 1 (severe damage), and 0 (completely dissolved).

### Hydrolytic degradation tests

For the hydrolytic degradation test, the films were cut into 2 × 2 cm<sup>2</sup> pieces and placed in 3% aqueous sodium hydroxide solutions at 45 °C. Specimens were retrieved after various lengths of time (on the order of days), rinsed with distilled

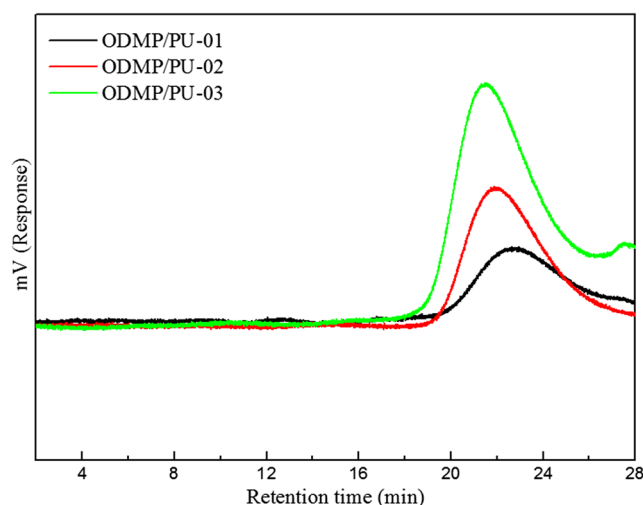


**Fig. 3** GPC curves of the ODMP/PUs

**Table 2** GPC result of ODMP/PUs

| Sample     | Retention time of the peak (min) | $\overline{Mn}$ ( $\times 10^4$ ) | $\overline{Mw}$ ( $\times 10^4$ ) | $\overline{Mw} / \overline{Mn}$ |
|------------|----------------------------------|-----------------------------------|-----------------------------------|---------------------------------|
| ODMP/PU-01 | 22.2                             | 1.70                              | 3.32                              | 2.0                             |
| ODMP/PU-02 | 21.4                             | 2.30                              | 4.32                              | 1.9                             |
| ODMP/PU-03 | 20.1                             | 3.85                              | 6.01                              | 1.6                             |

water, and placed in a vacuum oven at 70 °C for 3 h. Hydrolytic degradation was then calculated according to specimen weight loss:

$$\text{Weight loss} = \frac{W_0 - W_t}{W_0} \times 100\% \quad (3)$$

where  $W_0$  is the dry weight prior to the degradation test and  $W_t$  is the dry weight at time  $t$ . The dimensions of the specimen were  $2 \times 2 \text{ cm}^2$ .

Scanning electron microscopy (SEM; Hitachi, Model number: SU151) was employed to observe the appearance of the specimens before and after hydrolysis. The specimens were cut into  $2 \times 2 \text{ cm}^2$  pieces and adhered to a round stage using carbon conductive tape. A thin plate of gold was applied to the specimens to improve resolution. The shooting magnification was 2.00 K.

### Erythrocyte adhesion experiments

After two centrifugations, human erythrocyte concentrate ( $35 \text{ cm}^3$ ) was obtained from whole blood ( $250 \text{ cm}^3$ ). The blood was provided by the Taoyuan Blood Donation Center. The human erythrocyte concentrate was oscillated at a frequency of 72 times per minutes and stored at 20–24 °C for later use in the blood compatibility testing of the specimens. A HEPES-Tyrodes buffer solution was prepared. The specimens were cut into small squares ( $5 \times 5 \text{ mm}^2$ ) and sterilized for 40 min using an autoclave. The sterilized specimens were soaked in the HEPES-Tyrodes buffer solution for 24 h. The buffer solution was then removed. Approximately  $1 \text{ cm}^3$  of human erythrocyte concentrate was syringed onto the specimens and incubated at 37 °C in a 5%  $\text{CO}_2$  atmosphere for 6 h. The samples were then rinsed gently with HEPES-Tyrodes buffer solution, after which the adhered platelets were fixed with glutaraldehyde solution (2.5 vol% in HEPES-Tyrodes) for 30 min. The surfaces were then washed with HEPES-Tyrodes buffer, dehydrated with a series of ethanol/water mixtures of increasing ethanol concentration (30, 50, 70, 80, 90, and 95% ethanol, 10 min in each mixture). Subsequently, the specimens were soaked in 100% ethanol concentration for 30 min and dried using a freeze dryer. The morphology of the erythrocytes adhered to the specimens was observed using the aforementioned SEM device. The specimens were cut into  $2 \times 2 \text{ cm}^2$  pieces and taped to a round stage using carbon conductive

tape. A thin plate of gold was applied to the specimens to improve resolution. The shooting magnification was 2.00 K. The number of adhered erythrocytes per  $3600 \mu\text{m}^2$  was counted using SEM. Five different spots were randomly selected, and the number of erythrocytes averaged over these spots was taken as the result.

## Results and discussion

### GPC analysis

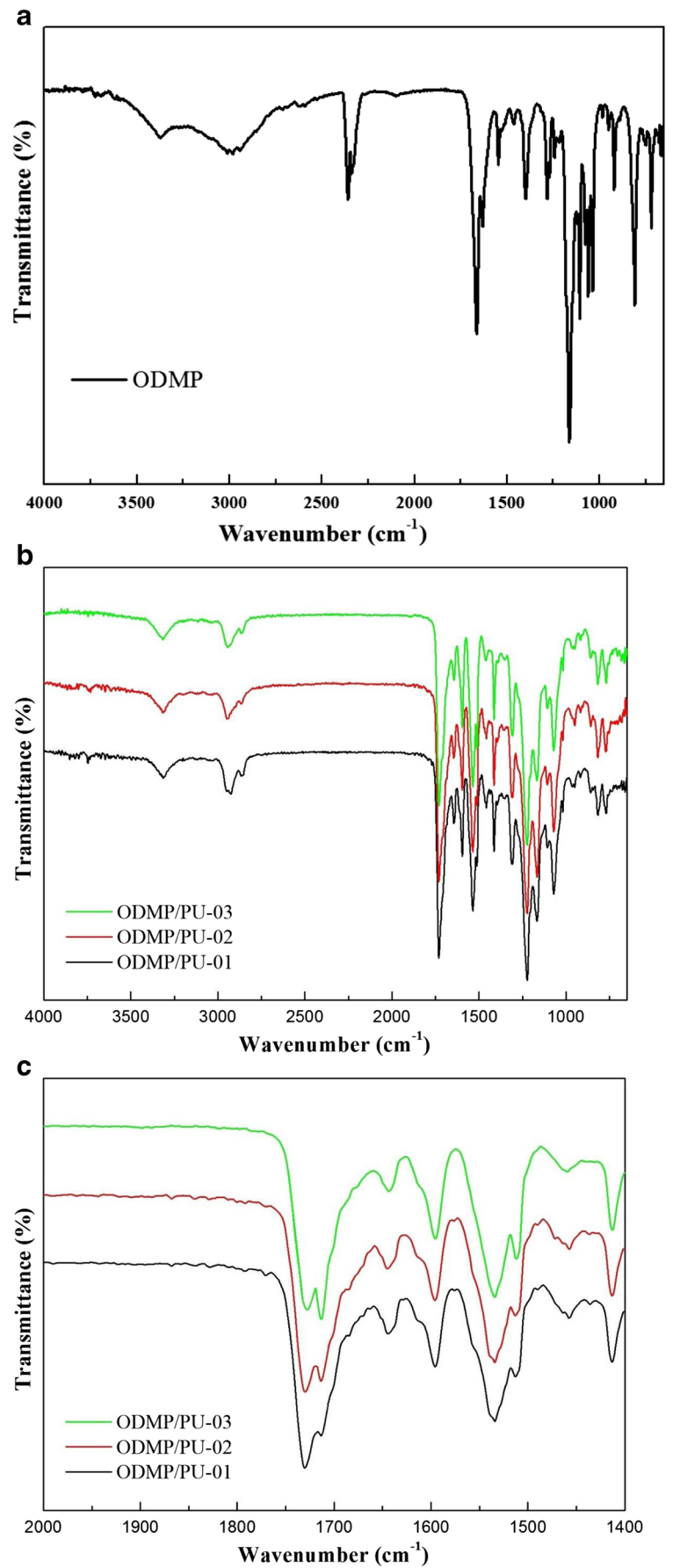
Fig. 3 presents the GPC curves of ODMP/PUs synthesized using different proportions of ODMP chain extender. The molecular weight distribution of these polymers was unimodal, no residual material was identified in these specimens. Table 2 presents the calculated  $\overline{Mw}/\overline{Mn}$  and reveals that the molecular weight of the ODMP/PUs increased when the ODMP content was increased. The  $\overline{Mw}/\overline{Mn}$ , i.e. the broadness of the molecular weight distributions, were in the range of 2.0–1.6. Higher ODMP chain extender content resulted in a narrower ODMP/PU molecular weight distribution. During the synthesis, increases in ODMP content elevated the viscosity of the polymer solution; therefore, higher ODMP chain extender content enhanced the molecular weight of the PUs.

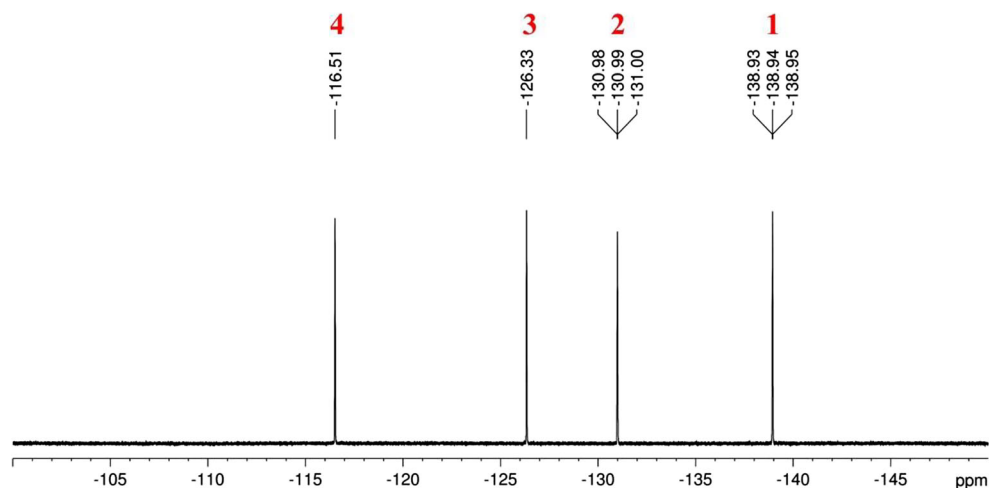
### FT-IR

The FT-IR spectrum of the ODMP chain extenders reveals a main absorption peak corresponding to hydroxyl groups ( $-\text{OH}$ ) at  $3367 \text{ cm}^{-1}$  and symmetrical and asymmetrical  $\text{CH}_2$  stretching vibration peaks at  $2937$  and  $2882 \text{ cm}^{-1}$ , respectively (Fig. 4[a]). The presence of these absorption peaks could be attributed to AMPD. ODMP structure formation can be inferred from several absorption peaks. Specifically, the peak at  $1664 \text{ cm}^{-1}$  indicates carbonyl groups ( $\text{C}=\text{O}$ ), the peak at  $1548 \text{ cm}^{-1}$  suggests  $\text{N}-\text{H}$  bending, and the peak at  $1284 \text{ cm}^{-1}$  corresponds to  $\text{C}-\text{N}$  stretching. Figs. 1 and 4(a) verify that ODMP chain extenders were successfully synthesized in this study.

Fig. 4(b) presents the FT-IR spectra of ODMP/PUs within the waveband  $4000\text{--}650 \text{ cm}^{-1}$ . Five main shared peaks are observed; the  $-\text{NH}$  stretching peak at  $3306 \text{ cm}^{-1}$ , the  $\text{CH}_2$  stretching peaks at  $2945$  and  $2861 \text{ cm}^{-1}$ , and peaks near

**Fig. 4** FT-IR spectra of the ODMP and ODMP/PUs at the wavenumber range of (a), (b) 4000–650  $\text{cm}^{-1}$ ; (b) 2000–1400  $\text{cm}^{-1}$

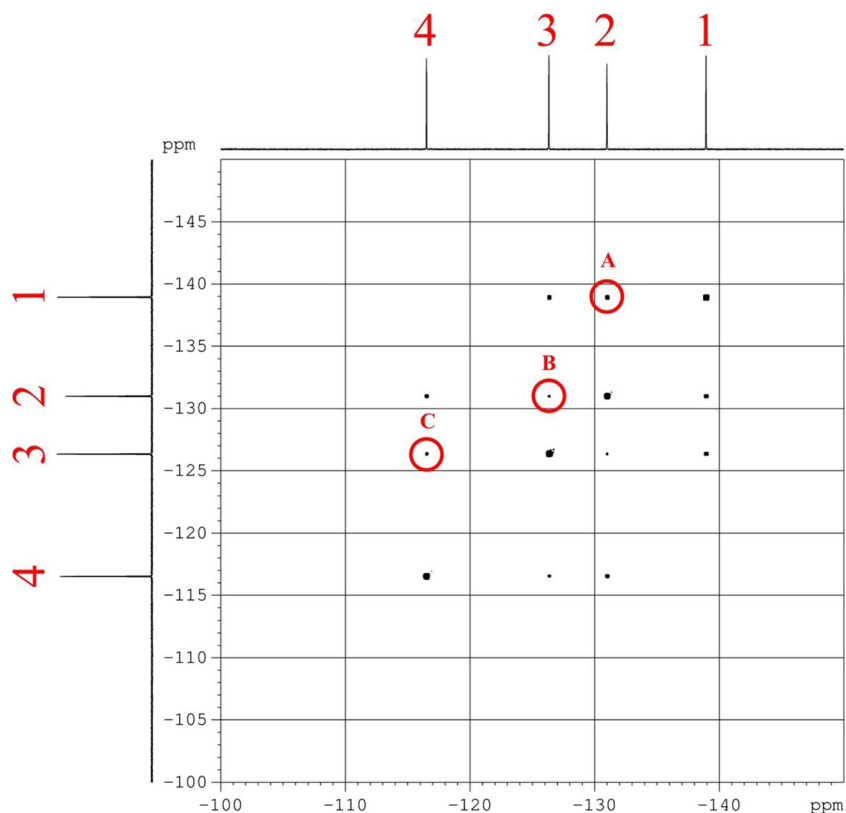


**Fig. 5**  $^{19}\text{F}$  NMR spectrum of the ODMP/PU-03

1729 and 1713  $\text{cm}^{-1}$  that represent carbonyl groups ( $\text{C}=\text{O}$ ). The peak at 1534  $\text{cm}^{-1}$  was due to the NH vibration of associated secondary urethane groups. The peaks at 1644 and 1595  $\text{cm}^{-1}$  suggest  $\text{C}=\text{C}$  stretching. The  $\text{C}-\text{F}$  and  $\text{C}-\text{O}$  groups stretching peaks are present at 1276 and 1222  $\text{cm}^{-1}$ , respectively. No free NCO group was observed between 2240 and 2275  $\text{cm}^{-1}$ . Thus, the MDI and ODMP chain extenders were fully reacted in the synthesis of MDI and PCL (Scheme 3).

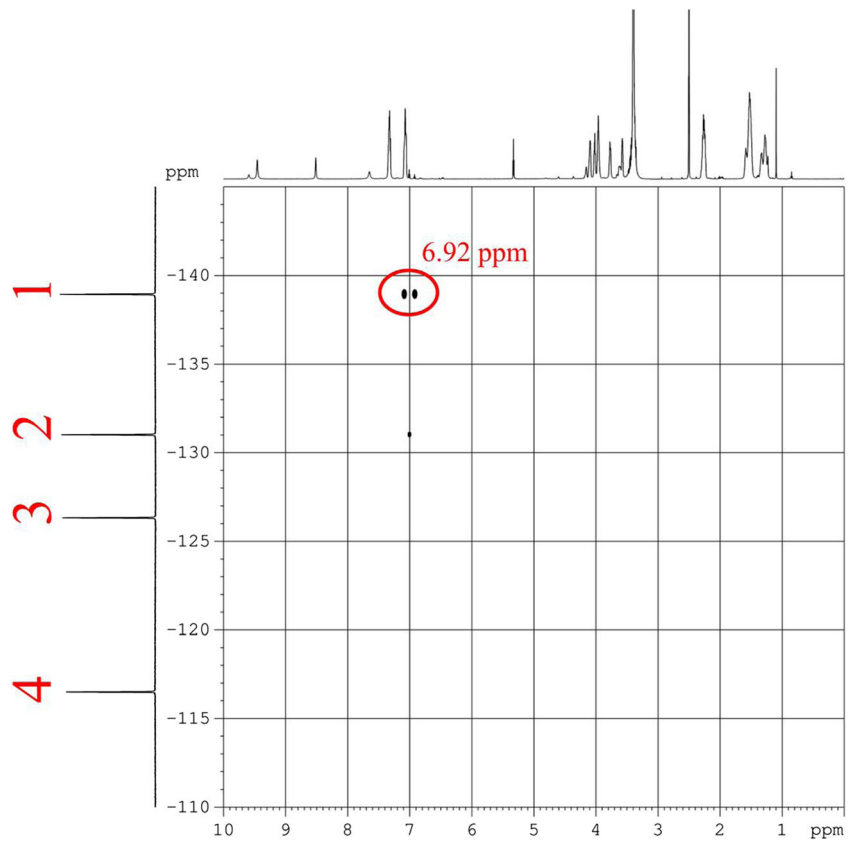
Fig. 4(c) presents the absorption peaks within the waveband 2000–1400  $\text{cm}^{-1}$ . Whereas the NH vibration peak of ODMP/PU-01 was located at 1534  $\text{cm}^{-1}$ , those

of ODMP/PU-02 and ODMP/PU-03 were located at lower wavenumbers of 1522 and 1514  $\text{cm}^{-1}$  respectively. This was caused by these polymers higher ODMP content, which triggered strong hydrogen bonding between  $-\text{NH}$  and  $\text{CF}_2$  groups [19, 20]. The 1729 and 1713  $\text{cm}^{-1}$  peaks were due to free and hydrogen-bonded  $\text{C}=\text{O}$  stretching, respectively. The spectra reveal that when the ODMP content was increased, the  $\text{C}=\text{O}$  peak shifted from 1729 to 1713  $\text{cm}^{-1}$  and the bonds were strengthened.  $\text{C}=\text{O}$  peaks shift to lower wavenumbers under the influence of a hydrogen bond [41]. Therefore, the  $\text{C}=\text{O}$  stretching shifted

**Fig. 6**  $^{19}\text{F}$ - $^{19}\text{F}$  COSY NMR spectrum of the ODMP/PU-03



**Fig. 7**  $^1\text{H}$ - $^{19}\text{F}$  COSY NMR spectrum of the ODMP/PU-03



to a lower wavelength because of the hydrogen bond interaction between the C = O and NH groups [42]. Higher ODMP content enabled this phenomenon to occur, specifically through strong interaction between the NH and CF<sub>2</sub> groups in ODMP/PU-02 and ODMP/PU-03.

**$^{19}\text{F}$  NMR**

Fig. 5 is the  $^{19}\text{F}$  NMR spectrum of ODMP/PU-03. Four absorption peaks are observed at -116.51, -126.33, -130.99, and -138.94 ppm. The four F valences were correspondingly

**Fig. 8** XPS survey spectra of the ODMP/PUs

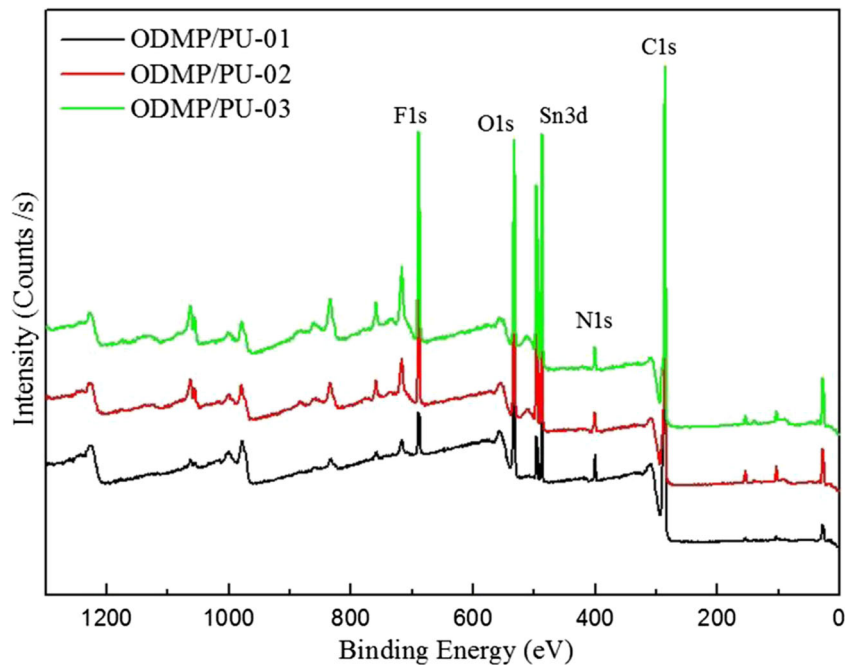


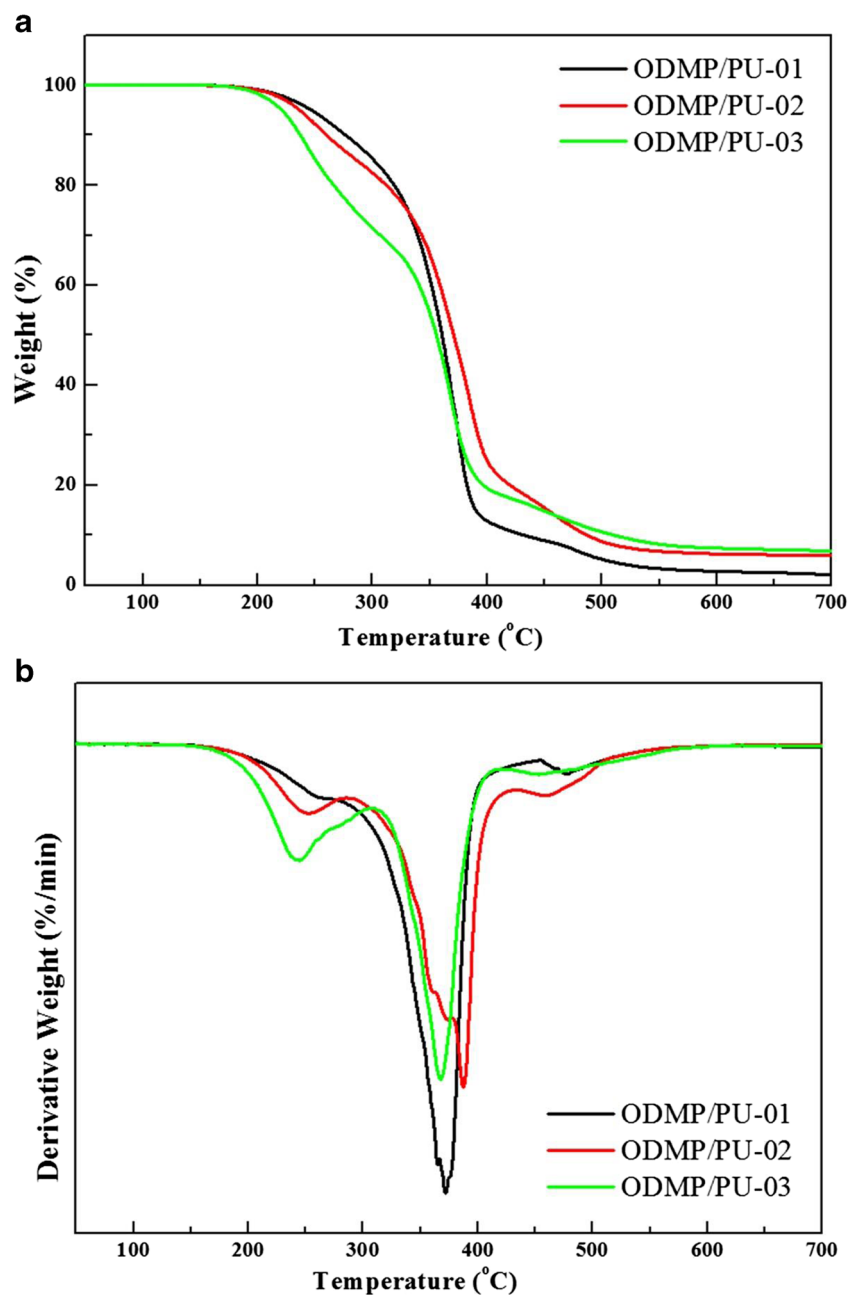
**Table 3** XPS peak characteristics of the ODMP/PUs

| Sample     |       | Binding energy (eV) | Atomic ratio (%) |
|------------|-------|---------------------|------------------|
| ODMP/PU-01 | C 1 s | 284.6               | 74.58            |
|            | O 1 s | 533.1               | 19.38            |
|            | N 1 s | 399.3               | 2.71             |
|            | F 1 s | 688.1               | 2.64             |
| ODMP/PU-02 | C 1 s | 284.1               | 70.60            |
|            | O 1 s | 533.1               | 17.56            |
|            | N 1 s | 399.6               | 2.94             |
|            | F 1 s | 687.4               | 6.80             |
| ODMP/PU-03 | C 1 s | 283.6               | 69.39            |
|            | O 1 s | 531.5               | 14.99            |
|            | N 1 s | 399.4               | 2.63             |
|            | F 1 s | 686.3               | 10.23            |

assigned as 1–4. Located between  $-110$  and  $-140$  ppm, these peaks are consistent with the typical range of  $CF_2$  signals [28–30].

To accurately assign absorption peaks 1–4 to the F valences of the molecular formula of ODMP/PU as F1, F2, F3, and F4, the  $^{19}F$ – $^{19}F$  correlation spectrum of ODMP/PU-03 was examined (Fig. 6). Three instances of strong couplings between next-nearest neighbors (i.e., F1–F2 [A], F2–F3 [B], and F3–F4 [C]) were observed.

Thus, the peaks located at  $-130.99$ ,  $-126.33$ ,  $-138.94$ , and  $-116.51$  ppm corresponded to F2, F3, F1, and F4, respectively. In addition, the  $^1H$ – $^{19}F$  correlation spectrum of ODMP/PU-03 reveals that the H atom at 6.92 ppm was adjacent to F1

**Fig. 9** TGA and DTG curves of the ODMP/PUs

**Table 4** Thermal properties of the ODMP/PUs

| Sample     | TGA                     |                          |                      | DSC                 |
|------------|-------------------------|--------------------------|----------------------|---------------------|
|            | T <sub>onset</sub> (°C) | T <sub>second</sub> (°C) | Residue at 700 °C(%) | T <sub>g</sub> (°C) |
| ODMP/PU-01 | 221.1                   | 337.7                    | 2.1                  | -22.1               |
| ODMP/PU-02 | 215.7                   | 343.6                    | 5.9                  | -20.3               |
| ODMP/PU-03 | 210.9                   | 347.6                    | 6.8                  | -18.4               |

(Fig. 7). Hence, the ODMP extenders successfully formed urethane groups with the MDI monomers.

## XPS

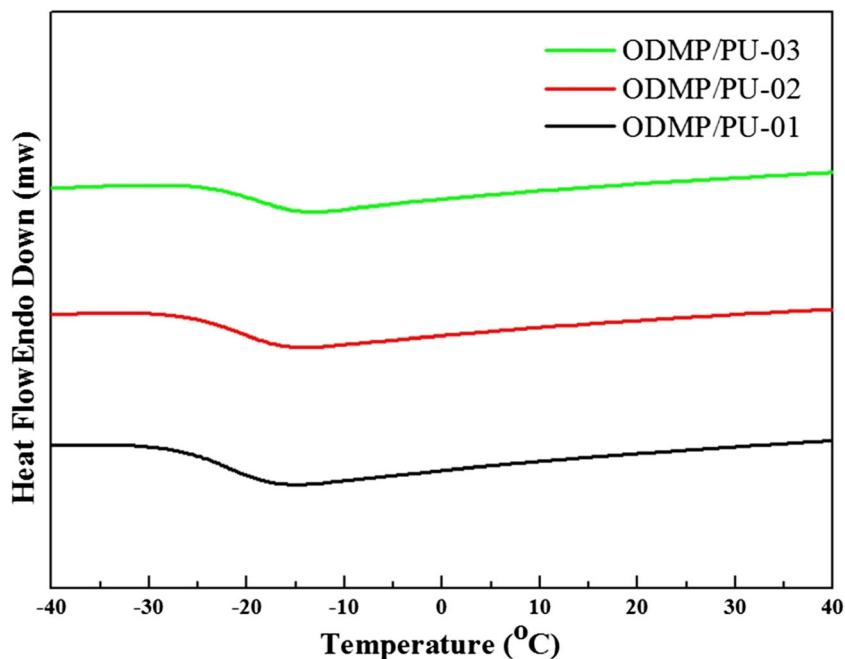
The elemental compositions and chemical state of the ODMP/PUs were determined using XPS. The XPS spectra of these polymers is shown in Fig. 8. Each polymer has four main peaks corresponding to the C 1 s, O 1 s, F 1 s, and N 1 s state orbits. In addition, another peak corresponds to the Sn 3d state orbit. The elemental compositions and associated peak characteristics are shown in Table 3.

The fluorine content of the ODMP/PUs was higher in polymers containing more ODMP chain extenders. Ferrara et al. [43] reported that in  $(-\text{CHFCH}_2-)_n$ , the binding energy of C 1 s in the  $\text{CH}_2$  group was 285.7 eV, and that of F 1 s in the CF group was 686.94 eV; and in the  $(-\text{CF}_2\text{CF}_2-)_n$  group, the binding energies of C 1 s and F 1 s were 292.48 and 689.67 eV, respectively. In this study, the binding energies of C 1 s in polymers ODMP/PU-01, ODMP/PU-02 and ODMP/PU-03 were 284.6, 284.1, and 283.6 eV, respectively, which are lower than the reported 292.48 eV of  $(-\text{CF}_2\text{CF}_2-)_n$ . Similarly, the corresponding binding energies of F 1 s in the

C–F bonds in ODMP/PU-01, ODMP/PU-02, and ODMP/PU-03 were 688.1, 687.4, and 686.3 eV, respectively, lower than that of the C–F bonds in fluorinated high-density polyethylene (689.67 eV) [43]. Thus, the binding energies of C 1 s and F 1 s were low, verifying the existence of interaction between -NH and  $\text{CF}_2$  groups in the ODMP/PUs. Related evidence was also presented in the previous discussion on the FT-IR spectra.

## Thermal properties

Fig. 9 presents TGA curves of ODMP/PUs containing various proportions of ODMP chain extenders. The first temperature indicated is the initial thermal decomposition temperature of the C–N group. Decomposition under high temperature is related to the decomposition of the urethane group, and the temperature at which this occurs was designated T<sub>second</sub>. The initial thermal decomposition temperatures of the PUs are listed in Table 4. The initial decomposition temperatures of ODMP/PU-01, ODMP/PU-02, and ODMP/PU-03 were 221.1, 215.7 and 210.9 °C, respectively. The T<sub>second</sub> of ODMP/PU-01, ODMP/PU-02, and ODMP/PU-03 were 337.7, 343.6 and 347.6 °C, respectively. The statistics in Table 4 indicate that the initial decomposition temperature

**Fig. 10** DSC thermograms of the ODMP/PUs

**Fig. 11** Dynamic mechanical analysis of the ODMP/PUs. **Tan  $\delta$**  (a), loss modulus ( $E''$ ) (b), storage modulus ( $E'$ ) (c)

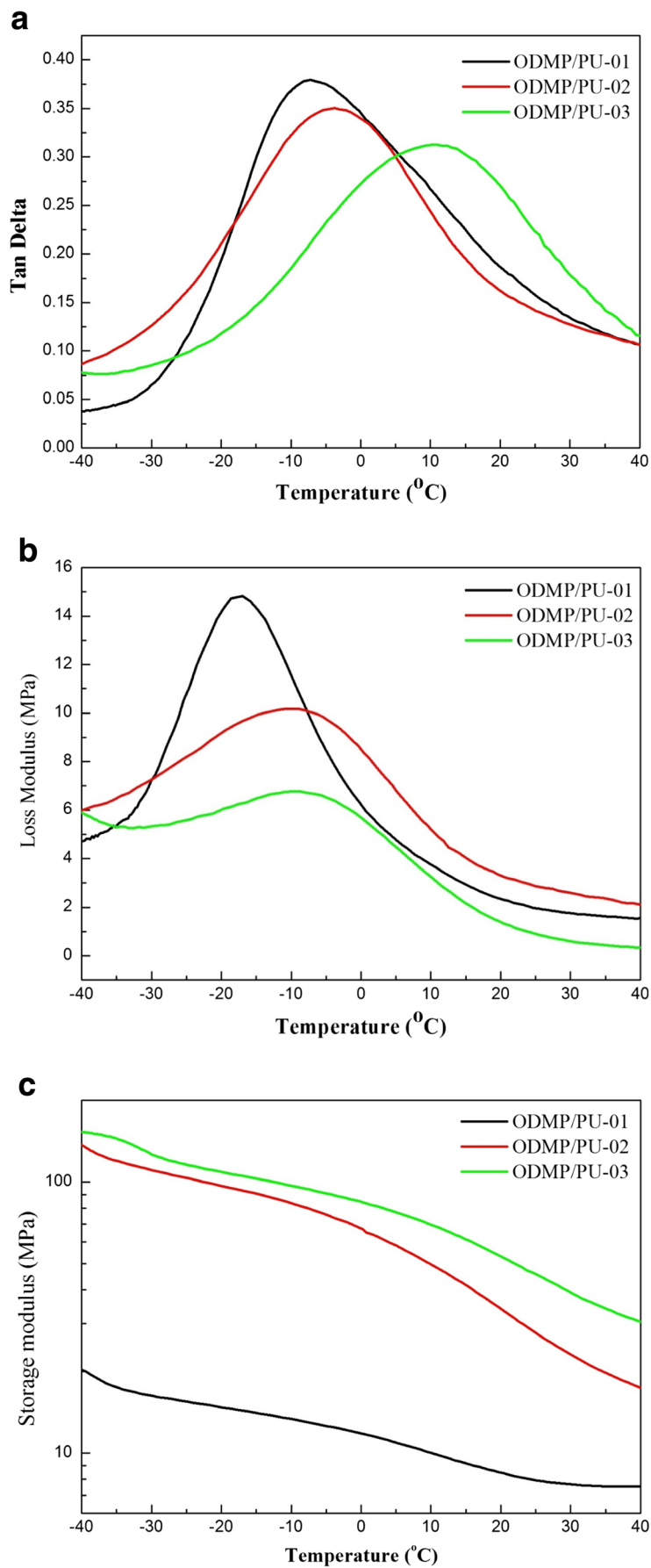


**Table 5** DMA results of the ODMP/PUs

| Sample     | Tgd from Tan $\delta$ (°C) | Tan $\delta_{\max}$ | Tgd from E'' (°C) | E'' <sub>max</sub> (MPa) | E' <sub>max</sub> at 25 °C (MPa) |
|------------|----------------------------|---------------------|-------------------|--------------------------|----------------------------------|
| ODMP/PU-01 | -7.2                       | 0.3794              | -17.0             | 14.8                     | 6.9                              |
| ODMP/PU-02 | -3.7                       | 0.3505              | -10.8             | 10.2                     | 15.6                             |
| ODMP/PU-03 | 10.3                       | 0.3124              | -8.7              | 6.8                      | 27.4                             |

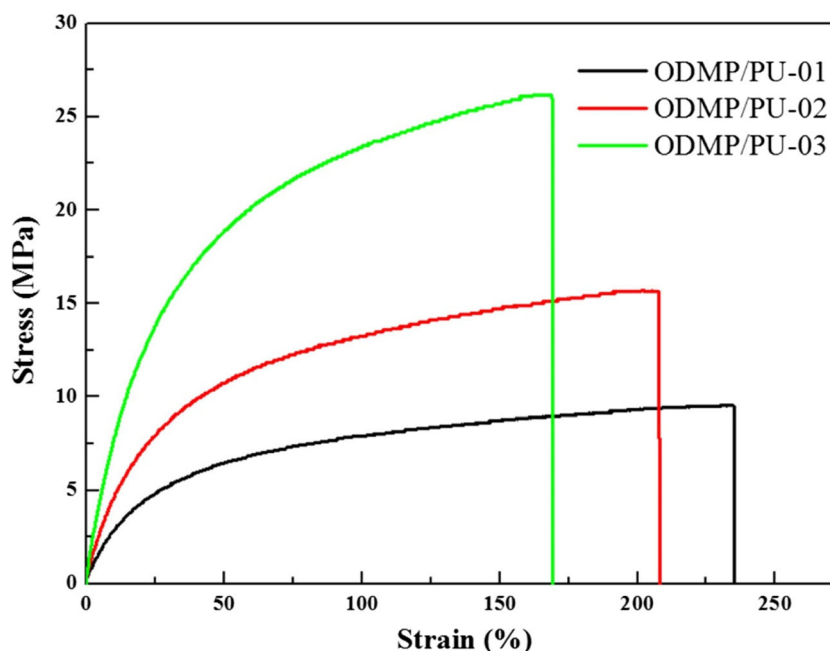
was decreased by more than 10 °C when the ODMP content was increased. This was due to the lower binding energy of the C–N bond in the main chain of ODMP/PU-03 (284 kJ/mol) compared with that of the C = O bond (799 kJ/mol). The observed increase in  $T_{\text{second}}$  when the ODMP content was increased can be attributed to the strong interactions between the -NH and CF<sub>2</sub> groups in the ODMP/PUs, as confirmed by the FT-IR and XPS analyses, and the fact that increasing the hard segment content generally affects the thermal stability of PUs. The results confirmed that the thermal stability of PUs is enhanced when the hard segment content or chain extender content is increased [29].

The DSC thermograms of ODMP/PUs with different ODMP content reveal that all ODMP/PUs attained a similar Tg, suggesting that both the soft and hard segments of the ODMP/PUs were in the homogeneous phase (Fig. 10) [44]. The Tg of ODMP/PU-01, ODMP/PU-02, and ODMP/PU-03 were -22.1, -20.3, and -18.4 °C, respectively (Table 4). Thus, increasing the ODMP content of the PUs enhanced their Tg. This phenomenon was expected because hard segments or chain extenders distribute evenly on the main chain of PUs and act as intrinsic fillers, thus elevating the glass transition temperature of the polymers. In addition, the FT-IR spectra

confirmed a strong interaction between the -NH and CF<sub>2</sub> groups in ODMP/PUs, which hindered the segmental motion of the ODMP/PUs and increased their glass transition temperature. The observed increase in Tg was similar to the TGA result, which indicated that the heat resistance of PUs is elevated when their ODMP content is increased.

### DMA

Fig. 11 presents the tan  $\delta$ , loss modulus (E'') and storage modulus curves of ODMP/PUs containing different proportions of ODMP chain extenders. The dynamic glass transition temperatures (Tgd) could be defined as tan  $\delta$  or the peak of the E'' curve. From the tan  $\delta$  curves, the dynamic glass transition temperatures of ODMP/PU-01, ODMP/PU-02, and ODMP/PU-03 were -7.2, -3.7, and 10.3 °C respectively. The Tgd of ODMP/PU-01, ODMP/PU-02, and ODMP/PU-03 as determined from the E'' curves were -17.0, -10.8, and -8.7 °C, respectively. Hence, different Tgd values were obtained using the different assessment methods (Table 5). The Tgd of the ODMP/PUs increased when the ODMP chain extender content was increased. This was consistent with the aforementioned DSC results. Due to strong interactions

**Fig. 12** Tensile properties of the ODMP/PUs

**Table 6** Tensile properties of the ODMP/PUs

| Sample     | Tensile strength (MPa) | Elongation at break (%) |
|------------|------------------------|-------------------------|
| ODMP/PU-01 | 9.57                   | 231                     |
| ODMP/PU-02 | 15.64                  | 203                     |
| ODMP/PU-03 | 26.31                  | 168                     |

between the -NH and CF<sub>2</sub> groups in the ODMP/PUs, the segmental motion of ODMP/PUs was hindered, which enhanced the Tgd of the polymers. PUs containing more ODMP achieved higher Tgd peaks in the tan  $\delta$  and E'' curves than PUs containing less ODMP. This was because higher ODMP content generated more hard segments, thus reducing the viscosity of the polymers. The loss modulus divided by the storage modulus equals tan  $\delta$ . Therefore, higher ODMP content decreased the loss modulus. Accordingly, the ODMP/PU with the highest ODMP content, ODMP/PU-03, obtained the lowest peak. Changes in the hard segment or chain extender content lowered the viscosity of the ODMP/PUs containing higher proportions of ODMP chain extenders. The storage modulus of ODMP/PUs at a fixed temperature increases with increasing ODMP content. For example, the storage moduli of these polymer at 25°C has the lowest value of 6.9 MPa of ODMP/PU-01 and ODMP/PU-03 has the highest value of 27.4 MPa.

### Tensile properties

Fig. 12 illustrates the stress–strain curves of ODMP/PUs containing different proportions of ODMP chain extenders. The tensile strengths of ODMP/PU-01, ODMP/PU-02, and ODMP/PU-03 were 9.57, 15.64, and 26.31 MPa, respectively (Table 6). Thus, increasing the ODMP content of the ODMP/PUs enhanced their tensile strength, possibly because it also increased their hard segment content. Adding either chain extenders or hard segments increases the tensile strength of PUs [27]. In addition, the strong interaction between the -NH and CF<sub>2</sub> groups in the ODMP/PUs hindered the polymers' segmental motion, thereby enhancing their tensile strength. The elongation at break of these three polymers were 231%, 203%, and 168% respectively (Table 6).

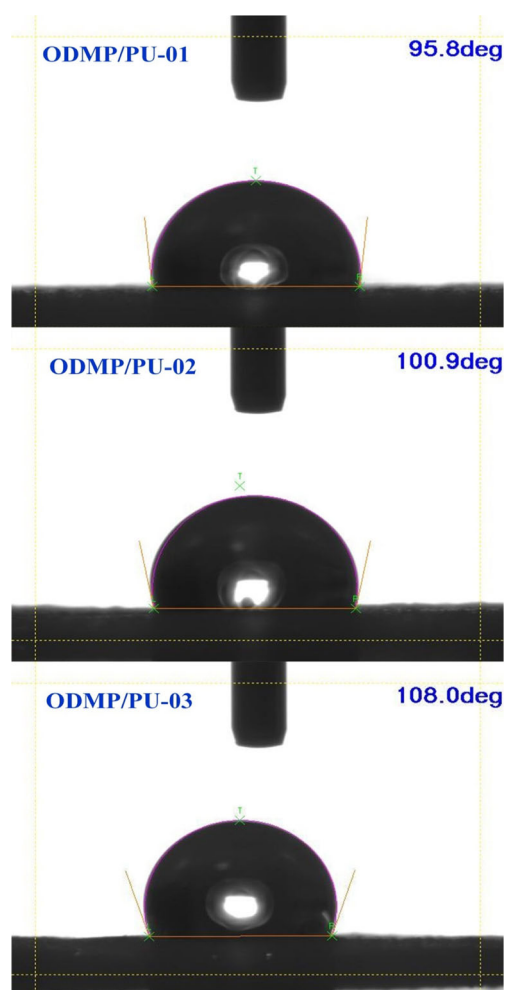
**Table 7** Density of adhered erythrocytes on the ODMP/PUs surfaces

| Sample     | No. of adhered erythrocytes (per 1000 $\mu\text{m}^2 \pm \text{S.D.}$ ) |
|------------|---|
| ODMP/PU-01 | aggregated  |
| ODMP/PU-02 | 72.6  |
| ODMP/PU-03 | 28.3  |

Therefore, increasing ODMP or hard segment content hindered the sliding motions among polymer chains. ODMP/PUs containing higher proportions of ODMP exhibited lower elongation at break. Also, the strong interaction between the CF<sub>2</sub> and -NH groups obstructed the motion of the polymer chains. Therefore, higher CF<sub>2</sub> or ODMP content resulted in the lower elongations at break of ODMP/PUs.

### Contact angle analysis

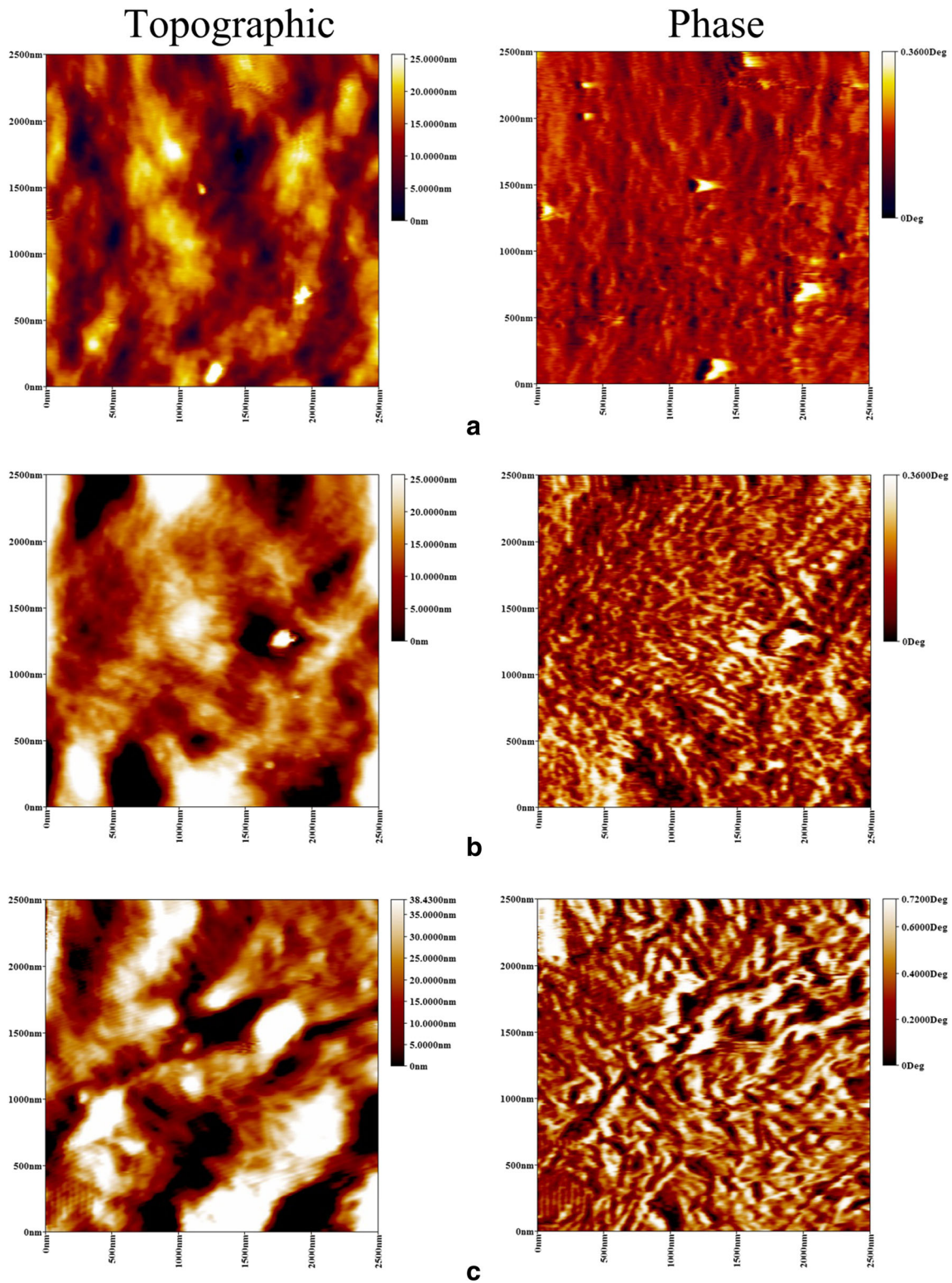
Fig. 13 presents pictures of the ODMP/PU contact angle tests. The surface activity of the ODMP/PUs was evaluated by their ability to be wetted by water. The contact angles obtained between water and ODMP/PU-01, ODMP/PU-02, and ODMP/PU-03 were 83.7°, 87.6°, and 90.2°, respectively. Therefore, the contact angle of water on the ODMP/PUs increased when their ODMP content was increased. Theoretically, the hydrophilic or hydrophobic properties of polymer surfaces are closely related to the chemical

**Fig. 13** Surface properties of the ODMP/PUs

compositions of those surfaces. Higher ODMP content also entailed lower PCL content and more fluorine units on the polymers surface. Thus, ODMP/PUs with higher ODMP content exhibited stronger hydrophobicity.

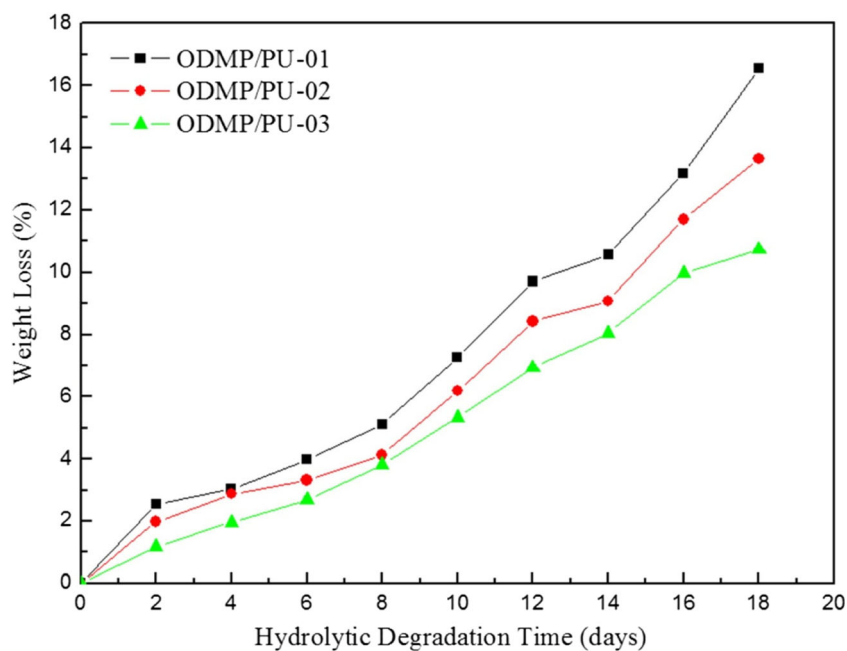
**Surface roughness analysis**

Fig. 14 presents the topography and phase data of ODMP/PU-01, ODMP/PU-02, and ODMP/PU-03. The surface



**Fig. 14** AFM topographic and phase images of the ODMP/PUs for (a) ODMP/PU-01, (b) ODMP/PU-02, and (c) ODMP/PU-03

**Fig. 15** Hydrolytic degradation results of the ODMP/PUs at 45 °C



topography reveals that all ODMP/PUs contained lumpy protrusions, and that those polymers with higher ODMP content had more conspicuous lumpy protrusions. The measured average roughness of the ODMP/PU-01, ODMP/PU-02, and

ODMP/PU-03 surfaces were 3.59, 5.28, and 9.70 nm, respectively. Thus, higher ODMP content rendered the PUs more rugged. The protrusions were caused by hard segments rich domains of the ODMP/PUs. The strong interaction between

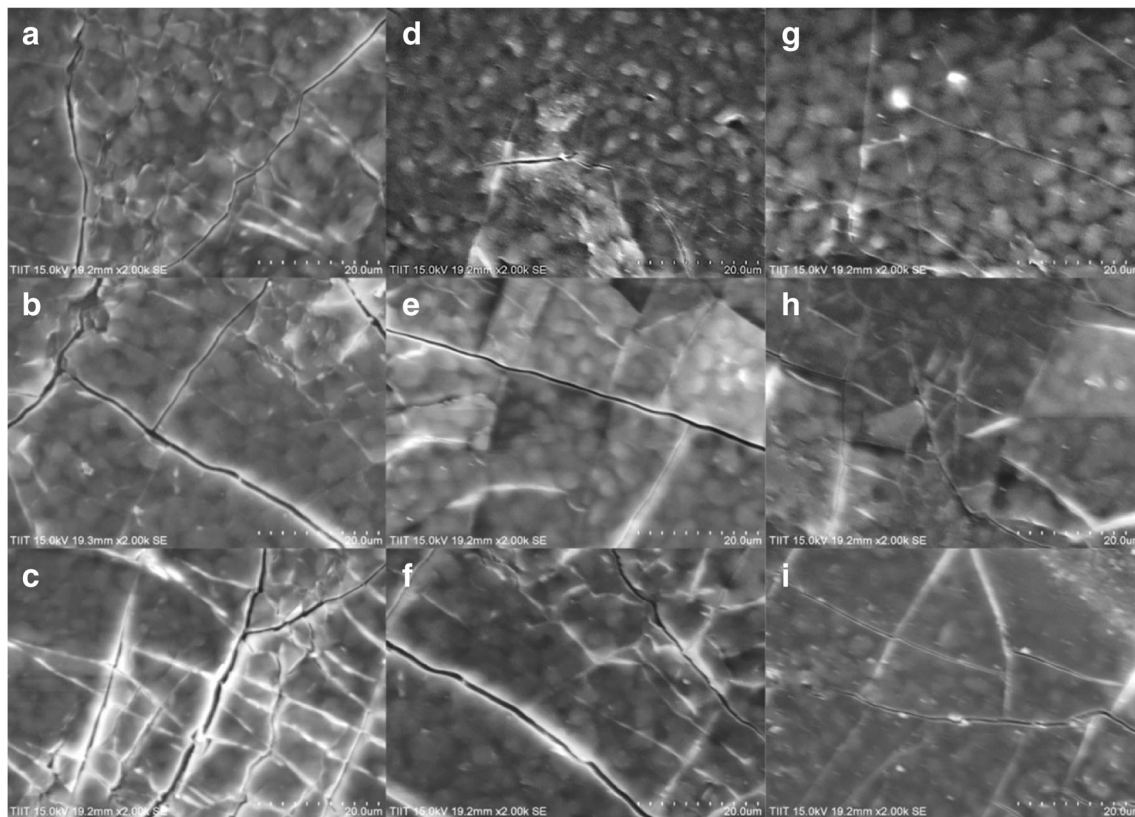
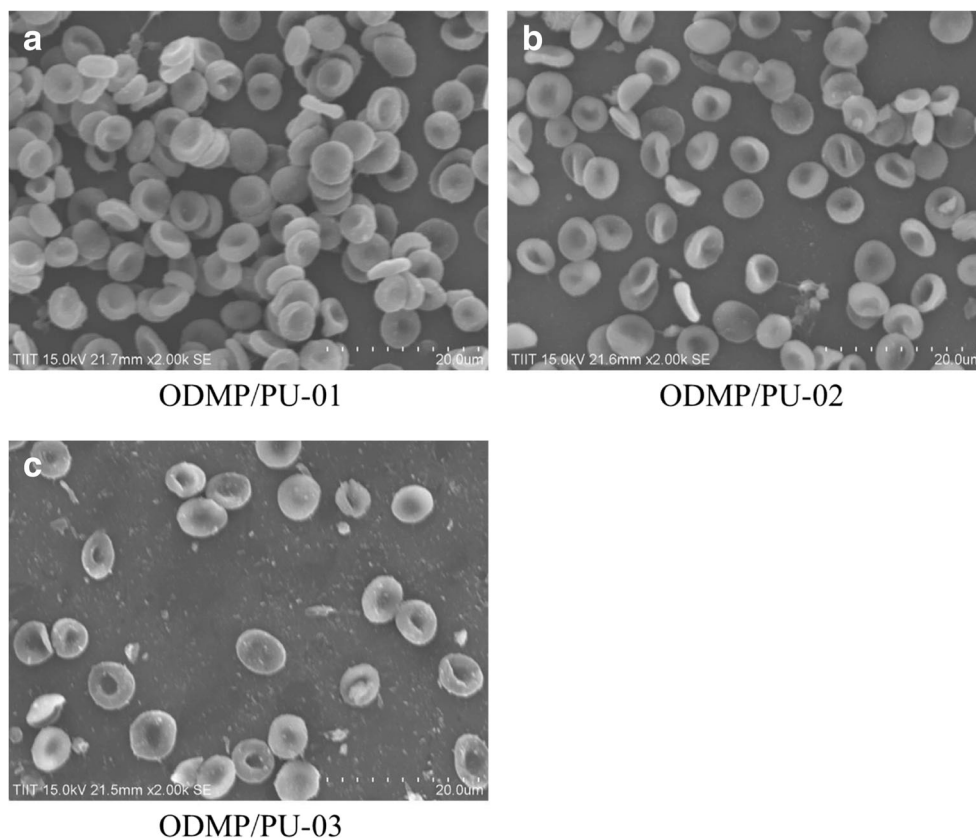


**Fig. 16** SEM micrographs of the (a) ODMP/PU-01, (d) ODMP/PU-02, and (g) ODMP/PU-03, with hydrolytic degradation for 6 d at 45 °C; (b) ODMP/PU-01, (e) ODMP/PU-02, and (h) ODMP/OF-03 with hydrolytic

degradation for 12 d at 45 °C; (c) ODMP/PU-01, (f) ODMP/PU-02, and (i) ODMP/PU-03 with hydrolytic degradation for 18 d at 45 °C



**Fig. 17** SEM micrographs of erythrocytes adhesion for (a) ODMP/PU-01, (b) ODMP/PU-02, and (c) ODMP/PU-03



the  $\text{CF}_2$  and  $-\text{NH}$  groups caused these aggregations on the film surfaces. The phase data of these fluorinated polymers indicated multiple irregular grainy or stripy phases, and polymers with higher ODMP content had more grainy or stripy phases. Therefore, grainy or stripy phases indicated that the ODMP chain extenders were in hard-segment-rich phases [45, 46].

### Hydrolytic degradation

Fig. 15 presents the results of the hydrolytic degradation of ODMP/PUs at 45 °C. In this test, the polymers were eroded under 3% aqueous NaOH solution. They lost weight over time. Polymers with higher ODMP chain extender content or lower PCL soft segment content exhibited greater hydrolytic degradation effect. Fluorinated polymers are resistant to hydrolytic degradation. To increase the degradability of polymers, PCL segment or nonfluorinated compound are more suitable.

Fig. 16 presents SEM micrographs of the ODMP/PUs after hydrolytic degradation at 45 °C for 6, 12, and 18 days. ODMP/PU-01 had larger and deeper cracks than ODMP/PU-02 or ODMP/PU-03. The cracks in ODMP/PU-01 grew even more obvious as the testing time was extended. Of the three polymers, ODMP/PU-01 contained the highest PCL content and ODMP/PU-03 had the lowest. Therefore, high PCL content facilitated the degradation of the polymers. Reducing PCL segment content or increasing fluorine or

ODMP chain extender content hinders the hydrolytic degradation of polymers.

### Erythrocyte adhesion results

When the surface of a material is exposed to blood, the adhesion and activity of erythrocytes can lead to the formation of thrombi. If a polymer material is to be used for biomedical purposes, the risk of thrombus formation must be minimal. In this study, an in vitro erythrocyte adhesion experiment was conducted as a preliminary assessment of the blood compatibility of the synthesized ODMP/PUs. Fig. 17 is an SEM image of erythrocyte concentrates on ODMP/PUs. Table 7 tabulates the average number of erythrocytes on the surface of each PU specimen. A substantial amount of erythrocytes clustered on the surface of ODMP/PU-01 and formed thrombi, rendering these erythrocytes innumerable. Therefore, using ODMP/PU-01 for biomedical purposes could induce severe thrombi. By comparison, the number of erythrocytes adhered on the surface of ODMP/PU-02 and ODMP/PU-03 were 72.6 and 28.3 no./1000  $\mu\text{m}^2$ , respectively, substantially fewer than on ODMP/PU-01. The average number of erythrocytes adhered on ODMP/PUs decreased as the ODMP chain extender or fluorine content was increased. Hence, the adhesion of fewer erythrocytes on the surface of ODMP/PU-02 and ODMP/PU-03 can be attributed to those polymers' increased fluorine content and decreased surface free energy. This finding is

valuable for those developing ODMP/PUs for use as biomedical materials.

## Conclusions

This study synthesized a novel fluoro chain extender ODMP using OFP and AMPD. PU prepolymers were synthesized using PCL and MDI. ODMP chain extenders were then added to prepare ODMP/PU polymers. The structure of ODMP and ODMP/PUs polymers was confirmed using  $^1\text{H}$  NMR,  $^{19}\text{F}$  NMR, and FT-IR. FT-IR and XPS demonstrated that there were strong interactions between the -NH and  $\text{CF}_2$  groups in the ODMP/PUs. Analysis of the polymers' thermal properties indicated that their heat resistance,  $T_g$ , and  $T_{gd}$  increased when their ODMP content was increased. In addition, an increase in ODMP content also resulted in the higher tensile strength, increased hydrophobicity, and better chemical resistance of the polymers. ODMP/PUs with lower ODMP chain extender content or higher PCL content exhibited higher hydrolytic degradation. Finally, results of an in vitro erythrocyte adhesion experiment revealed that increasing ODMP or fluorine content enhanced the thromboresistance of the PUs, thus widening their possible range of application in biomedical materials.

## References

- Ratna D, Karger-Kocsis J (2008) Recent advances in shape memory polymers and composites: a review. *J Mater Sci* 43:254–269
- Tien YI, Wei KH (2001) Hydrogen bonding and mechanical properties in segmented montmorillonite/polyurethane nanocomposites of different hard segment ratios. *Polymer* 42:3213–3221
- Abraham GA, de Queiroz AAA, San Roman JS (2001) Hydrophilic hybrid IPNs of segmented polyurethanes and copolymers of vinylpyrrolidone for applications in medicine. *Biomaterials* 22:1971–1985
- Mequanint K, Sanderson R (2003) Nano-structure phosphorus-containing polyurethane dispersions: synthesis and crosslinking with melamine formaldehyde resin. *Polymer* 44:2631–2639
- Park HB, Lee YM (2002) Separation of toluene/nitrogen through segmented polyurethane and polyurethane urea membranes with different soft segments. *J Membrane Sci* 197:283–296
- Gugliuzza A, Clarizia G, Golemme G, Drioli E (2002) New breathable and waterproof coatings for textiles: effect of an aliphatic polyurethane on the formation of PEEK-WC porous membranes. *Eur Polym J* 38:235–242
- Kawakami H, Mikawa M, Takagi J, Nagaoka S (1996) Gas transfer and blood compatibility of fluorinated polyimide membranes. *J Biomater Sci Polym Ed* 7:1029–1038
- Furukawa M (1994) Property-structure relationships of polyurethane elastomers: improvement of hydrolytic stability and thermal stability. *J Appl Polym Sci-Appl Polym Symp* 53:61–76
- Tonelli C, Trombetta T, Scicchitano M, Castiglioni G (1995) New perfluoropolyether soft segment containing polyurethanes. *J Appl Polym Sci* 57:1031–1042
- Sawada H (1996) Fluorinated peroxides. *Chem Rev* 96:1779–1808
- Sawada H, Ariyoshi Y, Lee L, Kyokane J, Kawase T (2000) A new approach to highly conductive polymer electrolytes: synthesis of gelling fluoroalkylated end-capped 2-acrylamido-2-methylpropanesulfonic acid copolymers containing poly(oxyethylene) units. *Eur Polym J* 36:2523–2526
- Ho T, Wynne KJ (1992) A new fluorinated polyurethane: polymerization, characterization, and mechanical properties. *Macromolecules* 25:3521–3527
- Honeychuck RV, Ho T, Wynne KJ, Nissan RA (1993) Preparation and characterization of polyurethanes based on a series of fluorinated diols. *Chem Mater* 5:1299–1306
- Su T, Wang GY, Wang SL, Hu CP (2010) Fluorinated siloxane-containing waterborne polyurethaneureas with excellent hemocompatibility, waterproof and mechanical properties. *Eur Polym J* 46:472–483
- Kashiwagi T, Ito Y, Imanishi Y (1993) Synthesis of non-thrombogenicity of fluoroalkyl poly-ether-urethanes. *J Biomater Sci Polym Ed* 5:157–166
- Wanga LF, Wei YH (2005) Effect of soft segment length on properties of fluorinated polyurethanes. *Colloid Surf B-Biointerfaces* 41:249–255
- Chen KY, Kuo JF (2000) Synthesis and properties of novel fluorinated aliphatic polyurethanes with fluoro chain extenders. *Macromol Chem Phys* 201:2676–2686
- Wang LF (2007) Experimental and theoretical characterization of the morphologies in fluorinated polyurethanes. *Polymer* 48:894–900
- Wu CL, Chiu SH, Lee HT, Suen MC (2016) Synthesis and properties of biodegradable polycaprolactone/polyurethanes using fluoro chain extenders. *Polym Adv Technol* 27:665–676
- Su SK, Gu JH, Lee HT, Yu SH, Wu CL, Suen MC (2016) Effects of an aromatic fluoro-diol and Polycaprolactone on the properties of the resultant polyurethanes. *Adv Polym Technol*. doi:10.1002/adv.21773
- Ge Z, Zhang XY, Dai JB, Li WH, Luo YJ (2008) Synthesis and characterization of fluorinated polyurethane with fluorine-containing pendent groups. *Chin Chem Lett* 19:1293–1296
- Ge Z, Zhang X, Dai J, Li W, Luo Y (2009) Synthesis, characterization and properties of a novel fluorinated polyurethane. *Eur Polym J* 45:530–536
- Tonelli C, Ajroldi G (2003) New fluoro-modified thermoplastic polyurethanes. *J Appl Polym Sci* 87:2279–2294
- Tonelli C, Trombetta T, Scicchitano M, Simeone G, Ajroldi G (1996) New fluorinated thermoplastic elastomers. *J Appl Polym Sci* 59:311–327
- Tonellia C, Ajroldi G, Turturro A, Marigo A (2001) Synthesis methods of fluorinated polyurethanes. 1. Effects on thermal and dynamic-mechanical behaviours. *Polymer* 42:5589–5598
- Tao L, Lin Y (2010) Synthesis and properties of fluorinated thermoplastic polyurethane elastomer. *J Fluor Chem* 131:36–41
- Mohanty AK, Misra M, Hinrichsen G (2000) Biofibres, biodegradable polymers and biocomposites: an overview. *Macromol Mater Eng* 276-277:1–24
- Mohanty AK, Misra M, Drzal LT (2002) Sustainable biocomposites from renewable resources: opportunities and challenges in the green materials world. *J Polym Environ* 10:19–26
- Gunatillake P, Mayadunne R, Adhikari R, El-Gewely MR (2006) Recent developments in biodegradable synthetic polymers. *Biotechnol Annu Rev* 12:301–347
- Pena J, Corrales T, Izquierdo-Barba I, Doadrio AL, Vallet-Regi M (2006) Long term degradation of poly( $\epsilon$ -caprolactone) films in biologically related fluids. *Polym Degrad Stab* 91:1424–1432
- Okada M (2002) Chemical syntheses of biodegradable polymers. *Prog Polym Sci* 27:87–133
- Nair LS, Laurencin CT (2007) Biodegradable polymers as biomaterials. *Prog Polym Sci* 32:762–798

33. Coulembier O, Degee P, Hedrick JL, Dubois P (2006) From controlled ring-opening polymerization to biodegradable aliphatic polyester: especially poly(b-malic acid) derivatives. *Prog Polym Sci* 31:723–747
34. Chandra R, Rustgi R (1998) Biodegradable polymers. *Prog Polym Sci* 23:1273–1335
35. Li FG, Hou JN, Zhu W, Zhang XA, Xu M, Luo XL (1996) Crystallinity and morphology of segmented polyurethanes with different soft-segment length. *J Appl Polym Sci* 62:631–638
36. Jeong HM, Ahn BK, Kim BK (2001) Miscibility and shape memory effect of thermoplastic polyurethane blends with phenoxy resin. *Eur Polym J* 37:2245–2252
37. Velankar S, Cooper SL (1998) Microphase separation and rheological properties of polyurethane melts. 1. Effect of block length. *Macromolecules* 31:9181–9192
38. Dadbin S, Frounchi M (2003) Effects of polyurethane soft segment and crosslink density on the morphology and mechanical properties of polyurethane/poly(allyl diglycol carbonate) simultaneous interpenetrating polymer networks. *J Appl Polym Sci* 89:1583–1595
39. Tsou CH, Lee HT, Tsai HA, Cheng HJ, Suen MC (2013) Synthesis and properties of biodegradable polycaprolactone/polyurethanes by using 2,6-pyridinedimethanol as a chain extender. *Polym Degrad Stab* 98:643–650
40. Jiang X, Li JH, Ding MM, Tan H, Ling QY, Zhong YP (2007) Synthesis and degradation of nontoxic biodegradable waterborne polyurethanes elastomer with poly( $\epsilon$ -caprolactone) and poly(ethylene glycol) as soft segment. *Eur Polym J* 43:1838–1846
41. Brunette CM, Hsu SL, Macknight WJ (1982) Hydrogen-bonding properties of hard-segment model compounds in polyurethane block copolymers. *Macromolecules* 15:71–77
42. Chen SJ, Hu J, Zhuo HT, Yuen CW, Chan LK (2010) Study on the thermal-induced shape memory effect of pyridine containing supramolecular polyurethane. *Polymer* 51:240–248
43. Ferrara AM, Silva JDL, Rego AMB (2003) XPS studies of directly fluorinated HDPE: problems and solutions. *Polymer* 44:7241–7249
44. Arun Prasath R, Nanjundan S, Pakula T, Klapper M (2004) Thermal and dynamic mechanical behaviour of calcium containing co-polyurethanes. *Polym Degrad Stabil* 85:911–923
45. Brandsch R, Bar G, Whangbo MH (1997) On the factors affecting the contrast of height and phase images in tapping mode atomic force microscopy. *Langmuir* 13:6349–6353
46. Sauer BB, Mclean RS, Thomas RR (1998) Tapping mode AFM studies of Nano-phases on fluorine-containing polyester coatings and Octadecyltrichlorosilane monolayers. *Langmuir* 14:3045–3051